

A MULTISCALE FINITE ELEMENT METHOD FOR AN ELLIPTIC DISTRIBUTED OPTIMAL CONTROL PROBLEM WITH ROUGH COEFFICIENTS AND CONTROL CONSTRAINTS

SUSANNE C. BRENNER, JOSÉ C. GARAY, AND LI-YENG SUNG

ABSTRACT. We construct and analyze a multiscale finite element method for an elliptic distributed optimal control problem with pointwise control constraints, where the state equation has rough coefficients. We show that the performance of the multiscale finite element method is similar to the performance of standard finite element methods for smooth problems and present corroborating numerical results.

1. INTRODUCTION

Let $\Omega \subset \mathbb{R}^d$ ($d = 1, 2, 3$) be a polytopal domain, $y_d \in L_2(\Omega)$ and $\gamma \leq 1$ be a positive constant. The model optimal control problem (cf. [27, 36]) is to find

$$(1.1) \quad (\bar{y}, \bar{u}) = \operatorname{argmin}_{(y,u) \in \mathbb{K}} J(y, u),$$

where the cost function $J : H_0^1(\Omega) \times L_2(\Omega) \rightarrow [0, \infty)$ is defined by

$$(1.2) \quad J(y, u) = \frac{1}{2} (\|y - y_d\|_{L_2(\Omega)}^2 + \gamma \|u\|_{L_2(\Omega)}^2),$$

the closed convex subset \mathbb{K} of $H_0^1(\Omega) \times L_2(\Omega)$ is defined by the conditions

$$(1.3) \quad a(y, z) = \int_{\Omega} uz \, dx \quad \forall z \in H_0^1(\Omega),$$

$$(1.4) \quad \phi_1 \leq u \leq \phi_2 \quad \text{a.e. in } \Omega,$$

and the bilinear form $a(\cdot, \cdot)$ is given by

$$(1.5) \quad a(y, z) = \int_{\Omega} \mathcal{A} \nabla y \cdot \nabla z \, dx.$$

We assume that the components of the symmetric positive definite matrix \mathcal{A} belong to $L_{\infty}(\Omega)$, and that there exist positive constants α and β such that

$$(1.6) \quad \text{the eigenvalues of } \mathcal{A} \text{ are bounded below (resp., above) by } \alpha \text{ (resp., } \beta).$$

Date: September 11, 2023.

2020 Mathematics Subject Classification. 65N30, 65N55, 65K10, 49M41, 35B27.

Key words and phrases. elliptic optimal control, rough coefficients, pointwise control constraints, multiscale finite element method, localized orthogonal decomposition, domain decomposition.

This work was supported in part by the National Science Foundation under Grant No. DMS-19-13035 and Grant No. DMS-22-08404.

For the constraint functions ϕ_1 and ϕ_2 , we assume

$$(1.7) \quad \phi_1 \text{ and } \phi_2 \text{ belong to } H^1(\Omega),$$

and

$$(1.8) \quad \phi_1 \leq \phi_2 \text{ a.e. on } \Omega.$$

Remark 1.1. Throughout this paper we follow the standard notation for differential operators, functions spaces and norms that can be found for example in [12, 1, 7].

Remark 1.2. The rough coefficients in the title of the paper refer to the fact that (1.6) is the only assumption on the matrix \mathcal{A} . Under this assumption we have the relation

$$(1.9) \quad \alpha |v|_{H^1(\Omega)}^2 \leq \|v\|_a^2 = a(v, v) \leq \beta |v|_{H^1(\Omega)}^2 \quad \forall v \in H^1(\Omega)$$

and nothing more. In particular, we do not assume the solution y of (1.3) belongs to $H^{1+s}(\Omega)$ for some positive s .

It is well-known that standard finite element methods for elliptic boundary value problems with rough coefficients can converge arbitrarily slowly (cf. [4]). This is of course also the case for the optimal control problem defined by (1.1)–(1.5). Our goal is to design a multiscale finite element method whose performance is in some sense similar to that of the standard finite element methods for smooth problems.

The literature on the numerical solution of this optimal control problem is relatively small. For problems with scale separations and periodic structures, the method in [28] is based on an asymptotic expansion of the solution, the method in [8] is based on the multiscale finite element space in [10], and the method in [18] is based on the heterogeneous multiscale method in [14]. For problems that do not assume scale separations or periodic structures, a numerical method based on the multiscale finite element space in [11] was investigated in [3], and a numerical method based on a generalization of the multiscale finite element space in [32] has just appeared in [9].

Our method is based on the local orthogonal decomposition (LOD) methodology (cf. [30]) which, like the methods in [3, 9], does not require scale separations or periodic structures in the coefficient matrix $\mathcal{A}(x)$. A variant of the LOD method for elliptic optimal control problems with rough coefficients but without control constraints can also be found in [6].

The rest of the paper is organized as follows. The properties of the continuous problem are recalled in Section 2 and a discretization of the optimal control problem is analyzed in Section 3, where we present error estimates that are convenient for the error analysis of multiscale finite element methods. The construction and analysis of our multiscale finite element method are presented in Section 4, followed by numerical results in Section 5. We end with some concluding remarks in Section 6.

2. THE CONTINUOUS PROBLEM

In this section we recall some well-known facts about the optimal control problem that can be found for example in [27, 36].

Since \mathbb{K} is nonempty under (1.8) and J is strictly convex and coercive, the minimization problem defined by (1.1)–(1.5) has a unique solution characterized by the first order optimality condition (cf. [25, 16])

$$(2.1) \quad \int_{\Omega} (\bar{y} - y_d)(y - \bar{y}) dx + \gamma \int_{\Omega} \bar{u}(u - \bar{u}) dx \geq 0 \quad \forall (y, u) \in \mathbb{K}.$$

Let the adjoint state $\bar{p} \in H_0^1(\Omega)$ be defined by

$$(2.2) \quad a(q, \bar{p}) = \int_{\Omega} (\bar{y} - y_d)q dx \quad \forall q \in H_0^1(\Omega).$$

One can use (1.3) and (2.2) to write

$$(2.3) \quad \int_{\Omega} (\bar{y} - y_d)y dx = a(y, \bar{p}) = \int_{\Omega} u\bar{p} dx \quad \forall (y, u) \in \mathbb{K},$$

and then (2.1) is equivalent to the inequality

$$(2.4) \quad \int_{\Omega} (\bar{p} + \gamma\bar{u})(u - \bar{u}) dx \geq 0 \quad \forall u \in K,$$

where

$$K = \{u \in L_2(\Omega) : \phi_1 \leq u \leq \phi_2 \text{ a.e. in } \Omega\}.$$

The inequality (2.4) is equivalent to the statement that \bar{u} is the $L_2(\Omega)$ -orthogonal projection of $-\gamma^{-1}\bar{p}$ on the closed convex subset K , i.e.,

$$(2.5) \quad \bar{u} = \max(\phi_1, \min(\phi_2, -\gamma^{-1}\bar{p})),$$

which, in view of (1.7), implies in particular that (cf. [19, Lemma 7.6])

$$\bar{u} \in H^1(\Omega).$$

For the analysis of problems with rough coefficients, it is desirable to keep track of the dependence of $|\bar{u}|_{H^1(\Omega)}$ on α and β . This can be achieved by using the estimate

$$\|\bar{y} - y_d\|_{L_2(\Omega)}^2 \leq 2J(y_*, u_*)$$

that holds for any convenient choice of $(y_*, u_*) \in \mathbb{K}$. One can then bound $|\bar{p}|_{H^1(\Omega)}$ through (2.2) and then obtain an estimate of $|\bar{u}|_{H^1(\Omega)}$ through (2.5).

For example, under the additional assumption $\phi_1 \leq 0 \leq \phi_2$ almost everywhere in Ω , we can take $(y_*, u_*) = (0, 0)$ to obtain a simple bound

$$(2.6) \quad \|\bar{y} - y_d\|_{L_2(\Omega)}^2 \leq 2J(0, 0) = \|y_d\|_{L_2(\Omega)}^2.$$

It then follows from (1.9), (2.2) and (2.6) that

$$\alpha|\bar{p}|_{H^1(\Omega)}^2 \leq a(\bar{p}, \bar{p}) = \int_{\Omega} (\bar{y} - y_d)\bar{p} dx \leq \|y_d\|_{L_2(\Omega)}\|\bar{p}\|_{L_2(\Omega)},$$

which implies

$$(2.7) \quad |\bar{p}|_{H^1(\Omega)} \leq (C_{PF}/\alpha)\|y_d\|_{L_2(\Omega)}$$

through the Poincaré-Friedrichs inequality

$$(2.8) \quad \|v\|_{L_2(\Omega)} \leq C_{PF}|v|_{H^1(\Omega)} \quad \forall v \in H_0^1(\Omega).$$

Putting (2.5) and (2.7) together, we arrive at the bound

$$|\bar{u}|_{H^1(\Omega)} \leq \max(|\phi_1|_{H^1(\Omega)}, |\phi_2|_{H^1(\Omega)}, \gamma^{-1}(C_{\text{PF}}/\alpha)\|y_d\|_{L_2(\Omega)}).$$

Remark 2.1. Under the general assumption (1.8), we can take $u_* = (\phi_1 + \phi_2)/2$ and obtain a (more complicated) upper bound for $|u|_{H^1(\Omega)}$ that depends only on $\|\phi_1\|_{H^1(\Omega)}$, $\|\phi_2\|_{H^1(\Omega)}$, $\|y_d\|_{L_2(\Omega)}$, γ^{-1} and α^{-1} .

Next we define

$$(2.9) \quad \lambda = \bar{p} + \gamma\bar{u}$$

and obtain through (2.5) the decomposition

$$(2.10) \quad \lambda = \lambda_1 + \lambda_2,$$

where

$$\lambda_1 = \max(\bar{p} + \gamma\phi_1, 0) \in H^1(\Omega) \quad \text{and} \quad \lambda_2 = \min(\bar{p} + \gamma\phi_2, 0) \in H^1(\Omega)$$

satisfy

$$(2.11a) \quad \lambda_1 \geq 0,$$

$$(2.11b) \quad \lambda_1(\phi_1 - \bar{u}) = 0,$$

$$(2.11c) \quad \nabla\lambda_1 = \begin{cases} \nabla\bar{p} + \gamma\nabla\phi_1 & \text{in } \mathfrak{A}_1 \\ 0 & \text{in } \Omega \setminus \mathfrak{A}_1 \end{cases},$$

$$(2.11d) \quad \lambda_2 \leq 0,$$

$$(2.11e) \quad \lambda_2(\phi_2 - \bar{u}) = 0,$$

$$(2.11f) \quad \nabla\lambda_2 = \begin{cases} \nabla\bar{p} + \gamma\nabla\phi_2 & \text{in } \mathfrak{A}_2 \\ 0 & \text{in } \Omega \setminus \mathfrak{A}_2 \end{cases}.$$

Here the active set \mathfrak{A}_j is the closure in Ω of the set of the Lebesgue points where $\bar{u} - \phi_j = 0$.

3. A DISCRETIZATION OF THE OPTIMAL CONTROL PROBLEM

Let \mathcal{T}_ρ be a simplicial/quadrilateral triangulation of Ω with mesh size ρ and $W_\rho \subset L_2(\Omega)$ be the space of piecewise constant functions with respect to \mathcal{T}_ρ . The optimal control \bar{u} will be approximated by functions in W_ρ , while the approximation of \bar{y} comes from a subspace V_* of $H_0^1(\Omega)$.

Remark 3.1. By allowing V_* to be an arbitrary subspace of $H_0^1(\Omega)$, the analysis developed below can be applied to standard finite element methods and multiscale finite element methods.

The discrete problem is to find

$$(3.1) \quad (\bar{y}_{*,\rho}, \bar{u}_{*,\rho}) = \underset{(y_*, u_\rho) \in \mathbb{K}_{*,\rho}}{\operatorname{argmin}} J(y_*, u_\rho),$$

where the closed convex subset $\mathbb{K}_{*,\rho}$ of $V_* \times W_\rho$ is defined by the following conditions:

$$(3.2) \quad a(y_*, z_*) = \int_{\Omega} u_\rho z_* dx \quad \forall z_* \in V_*,$$

$$(3.3) \quad Q_\rho \phi_1 \leq u_\rho \leq Q_\rho \phi_2 \quad \text{a.e. in } \Omega,$$

and Q_ρ is the orthogonal projection from $L_2(\Omega)$ onto W_ρ .

We have a standard interpolation error estimate (cf. [12, 7])

$$(3.4) \quad \|\zeta - Q_\rho \zeta\|_{L_2(\Omega)} \leq C_{\mathfrak{X}} \rho |\zeta|_{H^1(\Omega)},$$

where the positive constant $C_{\mathfrak{X}}$ only depends on the shape regularity of \mathcal{T}_ρ .

Since $Q_\rho u$ satisfies (3.3) for any u that satisfies (1.4), the set $\mathbb{K}_{*,\rho}$ is nonempty and the discrete convex minimization problem has a unique solution characterized by the first order optimality condition

$$(3.5) \quad \int_{\Omega} (\bar{y}_{*,\rho} - y_d)(y_* - \bar{y}_{*,\rho}) dx + \gamma \int_{\Omega} \bar{u}_{*,\rho}(u_\rho - \bar{u}_{*,\rho}) dx \geq 0 \quad \forall (y_*, u_\rho) \in \mathbb{K}_{*,\rho}.$$

The error analysis for $(\bar{y}_{*,\rho}, \bar{u}_{*,\rho})$ was carried out in the pioneering work [17] on finite element methods for elliptic optimal control problems. Here we present a self-contained treatment that is suitable for the analysis of the multiscale finite element method in Section 4.

The following lemma is useful for the error analysis.

Lemma 3.2. *Let $g \in L_2(\Omega)$ and $w_* \in V_*$ satisfy*

$$a(w_*, v_*) = \int_{\Omega} g v_* dx \quad \forall v_* \in V_*.$$

Then we have

$$(3.6) \quad \|w_*\|_{L_2(\Omega)} \leq (C_{\text{PF}}^2/\alpha) \|g\|_{L_2(\Omega)},$$

$$(3.7) \quad \|w_*\|_a \leq (C_{\text{PF}}/\sqrt{\alpha}) \|g\|_{L_2(\Omega)}.$$

Proof. It follows from (1.9), (2.8) and the Cauchy-Schwarz inequality that

$$\begin{aligned} \|w_*\|_{L_2(\Omega)}^2 &\leq C_{\text{PF}}^2 |w_*|_{H^1(\Omega)}^2 \leq (C_{\text{PF}}^2/\alpha) a(w_*, w_*) \\ &= (C_{\text{PF}}^2/\alpha) \int_{\Omega} g w_* dx \leq (C_{\text{PF}}^2/\alpha) \|g\|_{L_2(\Omega)} \|w_*\|_{L_2(\Omega)}, \end{aligned}$$

which implies (3.6).

The estimate (3.7) also follows from (1.9), (2.8) and the Cauchy-Schwarz inequality:

$$\|w_*\|_a^2 = a(w_*, w_*) = \int_{\Omega} g w_* dx \leq \|g\|_{L_2(\Omega)} \|w_*\|_{L_2(\Omega)} \leq \|g\|_{L_2(\Omega)} (C_{\text{PF}}/\sqrt{\alpha}) \|w_*\|_a.$$

□

We will include the approximation of \bar{p} by $\bar{p}_{*,\rho}$ in the error analysis, where $\bar{p}_{*,\rho} \in V_*$ is defined by

$$(3.8) \quad a(q_*, \bar{p}_{*,\rho}) = \int_{\Omega} (\bar{y}_{*,\rho} - y_d) q_* dx \quad \forall q_* \in V_*.$$

Theorem 3.3. *There exists a positive constant C_\dagger , depending only on $\|y_d\|_{L_2(\Omega)}$, $\|\phi_1\|_{H^1(\Omega)}$, $\|\phi_2\|_{H^1(\Omega)}$, γ^{-1} , α^{-1} and the shape regularity of \mathcal{T}_ρ , such that*

$$(3.9) \quad \|\bar{y} - \bar{y}_{*,\rho}\|_{L_2(\Omega)} + \|\bar{u} - \bar{u}_{*,\rho}\|_{L_2(\Omega)} + \|\bar{p} - \bar{p}_{*,\rho}\|_{L_2(\Omega)} \leq C_\dagger (\|\bar{y} - \dot{y}_*\|_{L_2(\Omega)} + \|\bar{p} - \dot{p}_*\|_{L_2(\Omega)} + \rho),$$

where $\dot{y}_*, \dot{p}_* \in V_*$ are defined by

$$(3.10) \quad a(\dot{y}_*, z_*) = \int_{\Omega} \bar{u} z_* dx \quad \forall z_* \in V_*,$$

$$(3.11) \quad a(q_*, \dot{p}_*) = \int_{\Omega} (\bar{y} - y_d) q_* dx \quad \forall q_* \in V_*.$$

Proof. First we note the following analog of (2.3):

$$(3.12) \quad \int_{\Omega} (\bar{y} - y_d) y_* dx = a(y_*, \dot{p}_*) = \int_{\Omega} u_{\rho} \dot{p}_* dx \quad \forall (y_*, u_{\rho}) \in \mathbb{K}_{*,\rho}$$

by (3.2) and (3.11).

Let $(\tilde{y}_*, \tilde{u}_{\rho}) \in \mathbb{K}_{*,\rho}$ be defined by

$$(3.13) \quad \tilde{u}_{\rho} = Q_{\rho} \bar{u}$$

and

$$(3.14) \quad a(\tilde{y}_*, z_*) = \int_{\Omega} \tilde{u}_{\rho} z_* dx \quad \forall z_* \in V_*.$$

It follows from (3.4) and (3.13) that

$$(3.15) \quad \|\bar{u} - \tilde{u}_{\rho}\|_{L_2(\Omega)} \leq C_{\star} \rho |\bar{u}|_{H^1(\Omega)}.$$

We have

$$(3.16) \quad \begin{aligned} & \|\bar{y} - \bar{y}_{*,\rho}\|_{L_2(\Omega)}^2 + \gamma \|\bar{u} - \bar{u}_{*,\rho}\|_{L_2(\Omega)}^2 \\ &= \int_{\Omega} (\bar{y} - \bar{y}_{*,\rho})(\bar{y} - \tilde{y}_*) dx + \gamma \int_{\Omega} (\bar{u} - \bar{u}_{*,\rho})(\bar{u} - \tilde{u}_{\rho}) dx \\ & \quad + \int_{\Omega} (\bar{y} - \bar{y}_{*,\rho})(\tilde{y}_* - \bar{y}_{*,\rho}) dx + \gamma \int_{\Omega} (\bar{u} - \bar{u}_{*,\rho})(\tilde{u}_{\rho} - \bar{u}_{*,\rho}) dx, \end{aligned}$$

and, in view of (2.9), (3.5) and (3.12),

$$(3.17) \quad \begin{aligned} & \int_{\Omega} (\bar{y} - \bar{y}_{*,\rho})(\tilde{y}_* - \bar{y}_{*,\rho}) dx + \gamma \int_{\Omega} (\bar{u} - \bar{u}_{*,\rho})(\tilde{u}_{\rho} - \bar{u}_{*,\rho}) dx \\ &= \int_{\Omega} \bar{y}(\tilde{y}_* - \bar{y}_{*,\rho}) dx + \gamma \int_{\Omega} \bar{u}(\tilde{u}_{\rho} - \bar{u}_{*,\rho}) dx \\ & \quad - \int_{\Omega} \bar{y}_{*,\rho}(\tilde{y}_* - \bar{y}_{*,\rho}) dx - \gamma \int_{\Omega} \bar{u}_{*,\rho}(\tilde{u}_{\rho} - \bar{u}_{*,\rho}) dx \\ &\leq \int_{\Omega} (\bar{y} - y_d)(\tilde{y}_* - \bar{y}_{*,\rho}) dx + \gamma \int_{\Omega} \bar{u}(\tilde{u}_{\rho} - \bar{u}_{*,\rho}) dx \\ &= \int_{\Omega} (\dot{p}_* + \gamma \bar{u})(\tilde{u}_{\rho} - \bar{u}_{*,\rho}) dx \\ &= \int_{\Omega} \lambda(\tilde{u}_{\rho} - \bar{u}_{*,\rho}) dx + \int_{\Omega} (\dot{p}_* - \bar{p})(\tilde{u}_{\rho} - \bar{u}_{*,\rho}) dx. \end{aligned}$$

We can bound the first integral on the right-hand side of (3.17) by (1.7), Remark 2.1, (2.10), (2.11), (3.3), (3.4) and (3.15):

$$\begin{aligned}
 \int_{\Omega} \lambda(\tilde{u}_{\rho} - \bar{u}_{*,\rho}) dx &= \int_{\Omega} \lambda_1(\tilde{u}_{\rho} - \bar{u}_{*,\rho}) dx + \int_{\Omega} \lambda_2(\tilde{u}_{\rho} - \bar{u}_{*,\rho}) dx \\
 &= \int_{\Omega} \lambda_1(Q_{\rho}\bar{u} - \bar{u}) dx + \int_{\Omega} \lambda_2(Q_{\rho}\bar{u} - \bar{u}) dx \\
 &\quad + \int_{\Omega} \lambda_1(\bar{u} - \phi_1) dx + \int_{\Omega} \lambda_2(\bar{u} - \phi_2) dx \\
 &\quad + \int_{\Omega} \lambda_1(\phi_1 - Q_{\rho}\phi_1) dx + \int_{\Omega} \lambda_2(\phi_2 - Q_{\rho}\phi_2) dx \\
 &\quad + \int_{\Omega} \lambda_1(Q_{\rho}\phi_1 - \bar{u}_{*,\rho}) dx + \int_{\Omega} \lambda_2(Q_{\rho}\phi_2 - \bar{u}_{*,\rho}) dx \\
 (3.18) \quad &\leq \int_{\Omega} \lambda_1(Q_{\rho}\bar{u} - \bar{u}) dx + \int_{\Omega} \lambda_2(Q_{\rho}\bar{u} - \bar{u}) dx \\
 &\quad + \int_{\Omega} \lambda_1(\phi_1 - Q_{\rho}\phi_1) dx + \int_{\Omega} \lambda_2(\phi_2 - Q_{\rho}\phi_2) dx \\
 &= \int_{\Omega} (\lambda_1 - Q_{\rho}\lambda_1)(Q_{\rho}\bar{u} - \bar{u}) dx + \int_{\Omega} (\lambda_2 - Q_{\rho}\lambda_2)(Q_{\rho}\bar{u} - \bar{u}) dx \\
 &\quad + \int_{\Omega} (\lambda_1 - Q_{\rho}\lambda_1)(\phi_1 - Q_{\rho}\phi_1) dx + \int_{\Omega} (\lambda_2 - Q_{\rho}\lambda_2)(\phi_2 - Q_{\rho}\phi_2) dx \\
 &\leq C_1\rho^2.
 \end{aligned}$$

For the second integral on the right-hand side of (3.17), we have

$$\begin{aligned}
 (3.19) \quad \int_{\Omega} (\dot{p}_* - \bar{p})(\tilde{u}_{\rho} - \bar{u}_{*,\rho}) dx &\leq \|\bar{p} - \dot{p}_*\|_{L_2(\Omega)} (\|\tilde{u}_{\rho} - \bar{u}\|_{L_2(\Omega)} + \|\bar{u} - \bar{u}_{*,\rho}\|_{L_2(\Omega)}) \\
 &\leq \|\bar{p} - \dot{p}_*\|_{L_2(\Omega)} (C_{\mathfrak{R}}\rho|\bar{u}|_{H^1(\Omega)} + \|\bar{u} - \bar{u}_{*,\rho}\|_{L_2(\Omega)})
 \end{aligned}$$

by (3.15).

It follows from Remark 2.1, (3.15), and (3.16)–(3.19) that

$$\begin{aligned}
 &\|\bar{y} - \bar{y}_{*,\rho}\|_{L_2(\Omega)}^2 + \gamma\|\bar{u} - \bar{u}_{*,\rho}\|_{L_2(\Omega)}^2 \\
 &\leq \|\bar{y} - \bar{y}_{*,\rho}\|_{L_2(\Omega)} \|\bar{y} - \tilde{y}_*\|_{L_2(\Omega)} + \gamma\|\bar{u} - \bar{u}_{*,\rho}\|_{L_2(\Omega)} C_{\mathfrak{R}}\rho|\bar{u}|_{H^1(\Omega)} \\
 &\quad + C_1\rho^2 + C_2\rho\|\bar{p} - \dot{p}_*\|_{L_2(\Omega)} + \|\bar{p} - \dot{p}_*\|_{L_2(\Omega)} \|\bar{u} - \bar{u}_{*,\rho}\|_{L_2(\Omega)},
 \end{aligned}$$

which together with the inequality of arithmetic and geometric means implies

$$(3.20) \quad \|\bar{y} - \bar{y}_{*,\rho}\|_{L_2(\Omega)} + \|\bar{u} - \bar{u}_{*,\rho}\|_{L_2(\Omega)} \leq C_3 (\|\bar{y} - \tilde{y}_*\|_{L_2(\Omega)} + \|\bar{p} - \dot{p}_*\|_{L_2(\Omega)} + \rho).$$

On the other hand, we have

$$a(\dot{y}_* - \tilde{y}_*, z_*) = \int_{\Omega} (\bar{u} - \tilde{u}_{\rho}) z_* dx \quad \forall z_h \in V_*,$$

by (3.10) and (3.14), and hence

$$(3.21) \quad \|\dot{y}_* - \tilde{y}_*\|_{L_2(\Omega)} \leq (C_{\text{PF}}^2/\alpha)\|\bar{u} - \tilde{u}_\rho\|_{L_2(\Omega)} \leq (C_{\text{PF}}^2/\alpha)C_{\star\rho}|\bar{u}|_{H^1(\Omega)}$$

by (3.4) and Lemma 3.2.

Putting (3.20) and (3.21) together, we arrive at the estimate

$$(3.22) \quad \|\bar{y} - \bar{y}_{*,\rho}\|_{L_2(\Omega)} + \|\bar{u} - \bar{u}_{*,\rho}\|_{L_2(\Omega)} \leq C_4(\|\bar{y} - \dot{y}_*\|_{L_2(\Omega)} + \|\bar{p} - \dot{p}_*\|_{L_2(\Omega)} + \rho).$$

For the estimate of $\bar{p} - \bar{p}_{*,\rho}$, we begin with

$$(3.23) \quad \|\bar{p} - \bar{p}_{*,\rho}\|_{L_2(\Omega)} \leq \|\bar{p} - \dot{p}_*\|_{L_2(\Omega)} + \|\dot{p}_* - \bar{p}_{*,\rho}\|_{L_2(\Omega)}$$

and note that

$$(3.24) \quad a(q_*, \dot{p}_* - \bar{p}_{*,\rho}) = \int_{\Omega} (\bar{y} - \bar{y}_{*,\rho})q_* dx \quad \forall q_* \in V_*$$

by (3.8) and (3.11), which implies

$$(3.25) \quad \|\dot{p}_* - \bar{p}_{*,\rho}\|_{L_2(\Omega)} \leq (C_{\text{PF}}^2/\alpha)\|\bar{y} - \bar{y}_{*,\rho}\|_{L_2(\Omega)}$$

through Lemma 3.2.

The estimate (3.9) follows from (3.22)–(3.25). \square

The following result shows that the estimate (3.9) is a tight estimate.

Theorem 3.4. *There exists a positive constant C_{\dagger} , depending only on α^{-1} , such that*

$$(3.26) \quad \|\bar{y} - \dot{y}_*\|_{L_2(\Omega)} + \|\bar{p} - \dot{p}_*\|_{L_2(\Omega)} \leq C_{\dagger}(\|\bar{y} - \bar{y}_{*,\rho}\|_{L_2(\Omega)} + \|\bar{u} - \bar{u}_{*,\rho}\|_{L_2(\Omega)} + \|\bar{p} - \bar{p}_{*,\rho}\|_{L_2(\Omega)}),$$

where \dot{y}_* (resp., \dot{p}_*) is defined by (3.10) (resp., (3.11)).

Proof. We have

$$(3.27) \quad \|\bar{y} - \dot{y}_*\|_{L_2(\Omega)} \leq \|\bar{y} - \bar{y}_{*,\rho}\|_{L_2(\Omega)} + \|\bar{y}_{*,\rho} - \dot{y}_*\|_{L_2(\Omega)},$$

and

$$a(\bar{y}_{*,\rho} - \dot{y}_*, z_*) = \int_{\Omega} (\bar{u}_{*,\rho} - \bar{u})z_* dx \quad \forall z_* \in V_*$$

by (3.2) and (3.10), which implies

$$(3.28) \quad \|\bar{y}_{*,\rho} - \dot{y}_*\|_{L_2(\Omega)} \leq (C_{\text{PF}}^2/\alpha)\|\bar{u} - \bar{u}_{*,\rho}\|_{L_2(\Omega)}$$

by Lemma 3.2.

Similarly we have

$$(3.29) \quad \begin{aligned} \|\bar{p} - \dot{p}_*\|_{L_2(\Omega)} &\leq \|\bar{p} - \bar{p}_{*,\rho}\|_{L_2(\Omega)} + \|\bar{p}_{*,\rho} - \dot{p}_*\|_{L_2(\Omega)} \\ &\leq \|\bar{p} - \bar{p}_{*,\rho}\|_{L_2(\Omega)} + (C_{\text{PF}}^2/\alpha)\|\bar{y} - \bar{y}_{*,\rho}\|_{L_2(\Omega)} \end{aligned}$$

by (3.25).

The estimate (3.26) follows from (3.27)–(3.29). \square

It is straightforward to derive error estimates in the energy norm from the estimate (3.9).

Theorem 3.5. *There exists a positive constant C_\S , depending only on $\|y_d\|_{L_2(\Omega)}$, $\|\phi_1\|_{H^1(\Omega)}$, $\|\phi_2\|_{H^1(\Omega)}$, γ^{-1} , α^{-1} and the shape regularity of \mathcal{T}_ρ , such that*

$$(3.30) \quad \|\bar{y} - \bar{y}_{*,\rho}\|_a + \|\bar{p} - \bar{p}_{*,\rho}\|_a \leq C_\S (\|\bar{y} - \dot{y}_*\|_a + \|\bar{p} - \dot{p}_*\|_a + \rho),$$

where $\dot{y}_*, \dot{p}_* \in V_*$ are defined in (3.10) and (3.11).

Proof. We have

$$(3.31) \quad \|\bar{y} - \bar{y}_{*,\rho}\|_a + \|\bar{p} - \bar{p}_{*,\rho}\|_a \leq \|\bar{y} - \dot{y}_*\|_a + \|\bar{p} - \dot{p}_*\|_a + \|\dot{y}_* - \bar{y}_{*,\rho}\|_a + \|\dot{p}_* - \bar{p}_{*,\rho}\|_a.$$

It follows from (3.2) and (3.10) that

$$a(\dot{y}_* - \bar{y}_{*,\rho}, z_*) = \int_{\Omega} (\bar{u} - \bar{u}_{*,\rho}) z_* dx \quad \forall z_* \in V_*,$$

and hence

$$(3.32) \quad \|\dot{y}_* - \bar{y}_{*,\rho}\|_a \leq (C_{\text{PF}}/\sqrt{\alpha}) \|\bar{u} - \bar{u}_{*,\rho}\|_{L_2(\Omega)}$$

by Lemma 3.2.

Similarly the relation (3.24) and Lemma 3.2 imply

$$(3.33) \quad \|\dot{p}_* - \bar{p}_{*,\rho}\|_a \leq (C_{\text{PF}}/\sqrt{\alpha}) \|\bar{y} - \bar{y}_{*,\rho}\|_{L_2(\Omega)}.$$

The estimate (3.30) is obtained by combining (3.9), (3.31)–(3.33) and the relation

$$\|\bar{y} - \dot{y}_*\|_{L_2(\Omega)} + \|\bar{p} - \dot{p}_*\|_{L_2(\Omega)} \leq (C_{\text{PF}}/\sqrt{\alpha}) (\|\bar{y} - \dot{y}_*\|_a + \|\bar{p} - \dot{p}_*\|_a)$$

that follows from (1.9) and (2.8). \square

Remark 3.6. Note that (2.2) and (3.11) imply $\dot{p}_* \in V_*$ is the projection of \bar{p} with respect to the bilinear form $a(\cdot, \cdot)$. Therefore we have

$$\|\bar{p} - \dot{p}_*\|_a = \inf_{q_* \in V_*} \|\bar{p} - q_*\|_a.$$

Similarly we have

$$\|\bar{y} - \dot{y}_*\|_a = \inf_{z_* \in V_*} \|\bar{y} - z_*\|_a$$

by (1.3) and (3.10).

Let $V_* = V_h$ be the P_1/Q_1 finite element space associated with a simplicial/quadrilateral triangulation \mathcal{T}_h of Ω with mesh size h and let $(\bar{y}_{*,\rho}, \bar{u}_{*,\rho}, \bar{p}_{*,\rho})$ be written as $(\bar{y}_{h,\rho}, \bar{u}_{h,\rho}, \bar{p}_{h,\rho})$. The estimate (3.9) becomes

$$(3.34) \quad \|\bar{y} - \bar{y}_{h,\rho}\|_{L_2(\Omega)} + \|\bar{u} - \bar{u}_{h,\rho}\|_{L_2(\Omega)} + \|\bar{p} - \bar{p}_{h,\rho}\|_{L_2(\Omega)} \leq C_\dagger (\|\bar{y} - \dot{y}_h\|_{L_2(\Omega)} + \|\bar{p} - \dot{p}_h\|_{L_2(\Omega)} + \rho),$$

where $\dot{y}_h, \dot{p}_h \in V_h$ are defined by

$$(3.35) \quad a(\dot{y}_h, z_h) = \int_{\Omega} \bar{u} z_h dx \quad \forall z_h \in V_h,$$

$$(3.36) \quad a(q_h, \dot{p}_h) = \int_{\Omega} (\bar{y} - y_d) q_h dx \quad \forall q_h \in V_h,$$

and the estimate (3.30) becomes

$$(3.37) \quad \|\bar{y} - \bar{y}_{h,\rho}\|_a + \|\bar{p} - \bar{p}_{h,\rho}\|_a \leq C_\S (\|\bar{y} - \dot{y}_h\|_a + \|\bar{p} - \dot{p}_h\|_a + \rho).$$

In the case where \mathcal{A} is the identity matrix and Ω is convex, we have $\bar{y}, \bar{p} \in H^2(\Omega)$ by the elliptic regularity theory for polygonal domains (cf. [20, 13, 31]). It follows from Remark 3.6, (3.34) and a standard duality argument (cf. [12, 7]) that

$$(3.38) \quad \|\bar{y} - \bar{y}_{h,\rho}\|_{L_2(\Omega)} + \|\bar{u} - \bar{u}_{h,\rho}\|_{L_2(\Omega)} + \|\bar{p} - \bar{p}_{h,\rho}\|_{L_2(\Omega)} \leq C(h^2 + \rho).$$

In this case the estimate (3.37) yields

$$(3.39) \quad |\bar{y} - \bar{y}_{h,\rho}|_{H^1(\Omega)} + |\bar{p} - \bar{p}_{h,\rho}|_{H^1(\Omega)} \leq C(h + \rho).$$

In the case of rough coefficients, we can derive from (2.8), (3.9), (3.30) and Remark 3.6 that

$$\begin{aligned} & \|\bar{y} - \bar{y}_{h,\rho}\|_{L_2(\Omega)} + \|\bar{u} - \bar{u}_{h,\rho}\|_{L_2(\Omega)} + \|\bar{p} - \bar{p}_{h,\rho}\|_{L_2(\Omega)} + \|\bar{y} - \bar{y}_{h,\rho}\|_a + \|\bar{p} - \bar{p}_{h,\rho}\|_a \\ & \leq C \left(\inf_{z_h \in V_h} \|\bar{y} - z_h\|_a + \inf_{q_h \in V_h} \|\bar{p} - q_h\|_a + \rho \right), \end{aligned}$$

which implies

$$\lim_{h,\rho \downarrow 0} \left(\|\bar{y} - \bar{y}_{h,\rho}\|_{L_2(\Omega)} + \|\bar{u} - \bar{u}_{h,\rho}\|_{L_2(\Omega)} + \|\bar{p} - \bar{p}_{h,\rho}\|_{L_2(\Omega)} + \|\bar{y} - \bar{y}_{h,\rho}\|_a + \|\bar{p} - \bar{p}_{h,\rho}\|_a \right) = 0.$$

However the convergence with respect to h can be very slow. Therefore a satisfactory approximate solution of the optimal control problem obtained by standard finite element methods will require a very fine mesh \mathcal{T}_h .

Below we will show that it is possible to recover on coarse meshes a performance similar to (3.38) and (3.39) for rough coefficients and general Ω provided that one takes a multiscale finite element space to be V_* .

4. A DD-LOD MULTISCALE FINITE ELEMENT METHOD

First we recall the construction of the multiscale finite element space from [5]. It begins with a simplicial/quadrilateral triangulation \mathcal{T}_H of Ω , and a refinement \mathcal{T}_h ($h \ll H$) of \mathcal{T}_H . The P_1/Q_1 finite element subspace of $H_0^1(\Omega)$ associated with \mathcal{T}_H (resp., \mathcal{T}_h) is denoted by V_H (resp., V_h).

The first step is to construct a projection operator $\Pi_H : H_0^1(\Omega) \rightarrow V_H$ such that

$$\frac{1}{H} \|v - \Pi_H v\|_{L_2(\Omega)} + |\Pi_H v|_{H^1(\Omega)} \leq C_b |v|_{H^1(\Omega)} \quad \forall v \in H_0^1(\Omega).$$

Remark 4.1. The operator Π_H in [5] is constructed by taking the averages of local L_2 projections. There are other constructions that are adapted to the coefficient matrix $\mathcal{A}(x)$ (cf. [33, 21]).

Let $K_h^{\Pi_H} = \{v \in V_h : \Pi_H v = 0\}$ be the kernel of Π_H in V_h and the correction operator $\mathcal{C}_h^{\Pi_H} : V_h \rightarrow K_h^{\Pi_H}$ be the projection operator with respect to $a(\cdot, \cdot)$, i.e.,

$$a(\mathcal{C}_h^{\Pi_H} v, w) = a(v, w) \quad \forall w \in K_h^{\Pi_H}.$$

The multiscale finite element space $V_H^{\text{ms,h}} \subset V_h$ is the orthogonal complement of $K_h^{\Pi_H}$ with respect to $a(\cdot, \cdot)$. Let ϕ_1, \dots, ϕ_m be the standard nodal basis functions of V_H associated with

the interior vertices p_1, \dots, p_m of \mathcal{T}_H . Then $V_H^{\text{ms,h}}$ is spanned by $\phi_1 - \mathcal{C}_h^{\Pi_H} \phi_1, \dots, \phi_m - \mathcal{C}_h^{\Pi_H} \phi_m$. The performance of the finite element method based on $V_H^{\text{ms,h}}$ for the problem

$$(4.1) \quad a(u, v) = \int_{\Omega} f v \, dx \quad \forall v \in H_0^1(\Omega)$$

with rough coefficients is similar to the performance of V_H for problems with smooth coefficients on convex domains (cf. [29, 30]). However, the construction of $V_H^{\text{ms,h}}$ requires solving m problems on the fine mesh \mathcal{T}_h , which is expensive.

The localized orthogonal decomposition (LOD) method is based on replacing the correction $\mathcal{C}_h^{\Pi_H} \phi_i$ by a correction computed in a subdomain consisting of a certain number of layers of elements from \mathcal{T}_H around p_i . It significantly reduces the computational cost and at the same time it preserves the good approximation property of $V_H^{\text{ms,h}}$ because the function $\mathcal{C}_h^{\Pi_H} \phi_i$ decays exponentially away from p_i (cf. [29, 30, 2]).

The multiscale finite element method from [5] is a variant of the LOD method which is based on the ideas in [26]. It computes an approximate solution $\mathcal{C}_{h,k}^{\Pi_H} \phi_i$ of the corrector equation

$$a(\mathcal{C}_h^{\Pi_H} \phi_i, w) = a(\phi_i, w) \quad \forall w \in K_h^{\Pi_H}$$

by applying k iterations of a preconditioned conjugate gradient (PCG) method with initial guess 0. The theory of PCG (cf. [34]) implies that the convergence of $\mathcal{C}_{h,k}^{\Pi_H} \phi_i$ to $\mathcal{C}_h^{\Pi_H} \phi_i$ in $\|\cdot\|_a$ is approximately q^k , where $q \in (0, 1)$ depends on the condition number of the preconditioned operator.

The key is to use an additive Schwarz domain decomposition preconditioner (cf. [35]) where the subdomains are small patches ω_i around p_i so that $\mathcal{C}_{h,k}^{\Pi_H} \phi_i$ is supported on a subdomain obtained by adding approximately $2k$ layers of elements from \mathcal{T}_H around ω_i , i.e., $\mathcal{C}_{h,k}^{\Pi_H} \phi_i$ is also a localized correction of ϕ_i . The computation of $\mathcal{C}_{h,k}^{\Pi_H} \phi_i$ only involves solving local small problems and $\|\mathcal{C}_h^{\Pi_H} \phi_i - \mathcal{C}_{h,k}^{\Pi_H} \phi_i\|_a = O(H)$ provided k is proportional to $|\ln H|$.

The multiscale finite element space $V_{H,k}^{\text{ms,h}} \subset V_h$ is spanned by $\phi_1 - \mathcal{C}_{h,k}^{\Pi_H} \phi_1, \dots, \phi_m - \mathcal{C}_{h,k}^{\Pi_H} \phi_m$. We will refer to it as the DD-LOD multiscale finite element space. The corresponding finite element method for (4.1) can be viewed as a reduced order method, where the functions $\mathcal{C}_{h,k}^{\Pi_H} \phi_1, \dots, \mathcal{C}_{h,k}^{\Pi_H} \phi_m$ are computed off-line. The on-line computation only involves solving an $m \times m$ system.

The following is the main result from [5] whose derivation only involves basic results from finite element methods, domain decomposition methods and numerical linear algebra.

Lemma 4.2. *Let $f \in L_2(\Omega)$, $y_h \in V_h$ and $y_{H,k}^{\text{ms,h}} \in V_{H,k}^{\text{ms,h}}$ such that*

$$\begin{aligned} a(y_h, z_h) &= \int_{\Omega} f z_h \, dx & \forall z_h \in V_h, \\ a(y_{H,k}^{\text{ms,h}}, z_{H,k}^{\text{ms,h}}) &= \int_{\Omega} f z_{H,k}^{\text{ms,h}} \, dx & \forall z_{H,k}^{\text{ms,h}} \in V_{H,k}^{\text{ms,h}}. \end{aligned}$$

There exists a positive constant C_{\sharp} depending on the shape regularity of \mathcal{T}_H but independent of α, β, h and H , such that

$$\|y_h - y_{H,k}^{\text{ms,h}}\|_a \leq (C_{\sharp}/\sqrt{\alpha})H\|f\|_{L_2(\Omega)},$$

$$\|y_h - y_{H,k}^{\text{ms},h}\|_{L_2(\Omega)} \leq (C_{\sharp}/\sqrt{\alpha})^2 H^2 \|f\|_{L_2(\Omega)},$$

provided $k = \lceil -j \ln H \rceil$ for a sufficiently large j .

Remark 4.3. The magnitude of j depends on the condition number of the preconditioned operator in the PCG algorithm.

The DD-LOD finite element method for (1.1)–(1.5) is defined by (3.1)–(3.3), where $V_* = V_{H,k}^{\text{ms},h}$ and its solution is denoted by $(\bar{y}_{H,k}^{\text{ms},h}, \bar{u}_\rho)$.

We also include the approximation of \bar{p} by $\bar{p}_{H,k}^{\text{ms},h}$ in the error analysis of the multiscale finite element method, where $\bar{p}_{H,k}^{\text{ms},h} \in V_{H,k}^{\text{ms},h}$ is defined by

$$(4.2) \quad a(q_{H,k}^{\text{ms},h}, \bar{p}_{H,k}^{\text{ms},h}) = \int_{\Omega} (\bar{y}_{H,k}^{\text{ms},h} - y_d) q_{H,k}^{\text{ms},h} dx \quad \forall q_{H,k}^{\text{ms},h} \in V_{H,k}^{\text{ms},h}.$$

Remark 4.4. Strictly speaking $\bar{y}_{H,k}^{\text{ms},h}$ and $\bar{p}_{H,k}^{\text{ms},h}$ also depend on ρ and \bar{u}_ρ also depends on h , H and k . These dependencies are suppressed for the sake of readability.

Theorem 4.5. *There exists a positive constant C_{\natural} , depending only on $\|y_d\|_{L_2(\Omega)}$, $\|\phi_1\|_{H^1(\Omega)}$, $\|\phi_2\|_{H^1(\Omega)}$, γ^{-1} , α^{-1} and the shape regularities of \mathcal{T}_H and \mathcal{T}_ρ , such that*

$$(4.3) \quad \|\bar{y} - \bar{y}_{H,k}^{\text{ms},h}\|_{L_2(\Omega)} + \|\bar{u} - \bar{u}_\rho\|_{L_2(\Omega)} + \|\bar{p} - \bar{p}_{H,k}^{\text{ms},h}\|_{L_2(\Omega)} \\ \leq C_{\natural} (\|\bar{y} - \bar{y}_{h,\rho}\|_{L_2(\Omega)} + \|\bar{u} - \bar{u}_{h,\rho}\|_{L_2(\Omega)} + \|\bar{p} - \bar{p}_{h,\rho}\|_{L_2(\Omega)} + H^2 + \rho),$$

where $(\bar{y}_{h,\rho}, \bar{u}_{h,\rho}, \bar{p}_{h,\rho})$ is the approximation of $(\bar{y}, \bar{u}, \bar{p})$ obtained by using the standard finite element space $V_h \times W_\rho$ in the discretization defined by (3.1)–(3.3).

Proof. We apply Theorem 3.3 (with $V_* = V_{H,k}^{\text{ms},h}$) to obtain

$$(4.4) \quad \|\bar{y} - \bar{y}_{H,k}^{\text{ms},h}\|_{L_2(\Omega)} + \|\bar{u} - \bar{u}_\rho\|_{L_2(\Omega)} + \|\bar{p} - \bar{p}_{H,k}^{\text{ms},h}\|_{L_2(\Omega)} \\ \leq C_{\dagger} (\|\bar{y} - \dot{y}_{H,k}^{\text{ms},h}\|_{L_2(\Omega)} + \|\bar{p} - \dot{p}_{H,k}^{\text{ms},h}\|_{L_2(\Omega)} + \rho),$$

where $\dot{y}_{H,k}^{\text{ms},h} \in V_{H,k}^{\text{ms},h}$ (resp., $\dot{p}_{H,k}^{\text{ms},h} \in V_{H,k}^{\text{ms},h}$) is the analog of \dot{y}_* in (3.10) (resp., \dot{p}_* in (3.11)), i.e., $\dot{y}_{H,k}^{\text{ms},h}$ is defined by

$$(4.5) \quad a(\dot{y}_{H,k}^{\text{ms},h}, z_{H,k}^{\text{ms},h}) = \int_{\Omega} \bar{u} z_{H,k}^{\text{ms},h} dx \quad \forall z_{H,k}^{\text{ms},h} \in V_{H,k}^{\text{ms},h},$$

and $\dot{p}_{H,k}^{\text{ms},h}$ is defined by

$$(4.6) \quad a(q_{H,k}^{\text{ms},h}, \dot{p}_{H,k}^{\text{ms},h}) = \int_{\Omega} (\bar{y} - y_d) q_{H,k}^{\text{ms},h} dx \quad \forall q_{H,k}^{\text{ms},h} \in V_{H,k}^{\text{ms},h}.$$

Let $\dot{y}_h \in V_h$ (resp., $\dot{p}_h \in V_h$) be defined by (3.35) (resp., (3.36)). According to Theorem 3.4, we have

$$(4.7) \quad \|\bar{y} - \dot{y}_h\|_{L_2(\Omega)} + \|\bar{p} - \dot{p}_h\|_{L_2(\Omega)} \leq C_{\ddagger} (\|\bar{y} - \bar{y}_{h,\rho}\|_{L_2(\Omega)} + \|\bar{u} - \bar{u}_{h,\rho}\|_{L_2(\Omega)} + \|\bar{p} - \bar{p}_{h,\rho}\|_{L_2(\Omega)}).$$

On the other hand, in view of Lemma 4.2, we have

$$(4.8) \quad \|\dot{y}_h - \dot{y}_{H,k}^{\text{ms},h}\|_{L_2(\Omega)} \leq (C_{\sharp}/\sqrt{\alpha})^2 H^2 \|\bar{u}\|_{L_2(\Omega)}$$

by (3.35) and (4.5), and

$$(4.9) \quad \|\dot{p}_h - \dot{p}_{H,k}^{\text{ms},h}\|_{L_2(\Omega)} \leq (C_{\#}/\sqrt{\alpha})^2 H^2 \|\bar{y} - y_d\|_{L_2(\Omega)}$$

by (3.36) and (4.6).

The estimate (4.3) follows from (4.4), (4.7)–(4.9) and the triangle inequality. \square

Remark 4.6. The estimate (4.3) indicates that up to an $O(H^2 + \rho)$ error the approximation of $(\bar{y}, \bar{u}, \bar{p})$ by $(\bar{y}_{H,k}^{\text{ms},h}, \bar{u}_{\rho}, \bar{p}_{H,k}^{\text{ms},h})$ is as good as the approximation by $(\bar{y}_{h,\rho}, \bar{u}_{h,\rho}, \bar{p}_{h,\rho})$. On the other hand, by comparing (3.38) and (4.3), we can also say that, up to the fine scale error, the performance of the multiscale finite element method on coarse meshes (with respect to the $L_2(\Omega)$ norm) is similar to the performance of standard finite element methods for problems with smooth coefficients on convex domains.

We also have error estimates in the energy norm.

Theorem 4.7. *There exists a positive constant C_{\diamond} , depending only on $\|y_d\|_{L_2(\Omega)}$, $\|\phi_1\|_{H^1(\Omega)}$, $\|\phi_2\|_{H^1(\Omega)}$, γ^{-1} , α^{-1} and the shape regularities of \mathcal{T}_H and \mathcal{T}_{ρ} , such that*

$$(4.10) \quad \|\bar{y} - \bar{y}_{H,k}^{\text{ms},h}\|_a + \|\bar{p} - \bar{p}_{H,k}^{\text{ms},h}\|_a \leq C_{\diamond} (\|\bar{y} - \bar{y}_{h,\rho}\|_a + \|\bar{p} - \bar{p}_{h,\rho}\|_a + H + \rho),$$

where $(\bar{y}_{h,\rho}, \bar{p}_{h,\rho})$ is the approximation of (\bar{y}, \bar{p}) obtained by using the standard finite element space $V_h \times W_{\rho}$ in the discretization defined by (3.1)–(3.3).

Proof. It follows from Theorem 3.5 that

$$(4.11) \quad \|\bar{y} - \bar{y}_{H,k}^{\text{ms},h}\|_a + \|\bar{p} - \bar{p}_{H,k}^{\text{ms},h}\|_a \leq C_{\S} (\|\bar{y} - \dot{y}_{H,k}^{\text{ms},h}\|_a + \|\bar{p} - \dot{p}_{H,k}^{\text{ms},h}\|_a + \rho),$$

where $\dot{y}_{H,k}^{\text{ms},h}, \dot{p}_{H,k}^{\text{ms},h} \in V_{H,k}^{\text{ms},h}$ are defined by (4.5) and (4.6).

Let $\dot{y}_h \in V_h$ (resp., $\dot{p}_h \in V_h$) be defined by (3.35) (resp., (3.36)). In view of Lemma 4.2, we have

$$(4.12) \quad \|\dot{y}_h - \dot{y}_{H,k}^{\text{ms},h}\|_a \leq (C_{\#}/\sqrt{\alpha})H \|\bar{u}\|_{L_2(\Omega)}$$

by (3.35) and (4.5), and also

$$(4.13) \quad \|\dot{p}_h - \dot{p}_{H,k}^{\text{ms},h}\|_a \leq C_{\#}/\sqrt{\alpha})H \|\bar{y} - y_d\|_{L_2(\Omega)}$$

by (3.36) and (4.6).

Finally we note that

$$(4.14) \quad \|\bar{y} - \dot{y}_h\|_a \leq \|\bar{y} - \bar{y}_{h,\rho}\|_a \quad \text{and} \quad \|\bar{p} - \dot{p}_h\|_a \leq \|\bar{p} - \bar{p}_{h,\rho}\|_a$$

by Remark 3.6.

The estimate (4.10) follows from (4.11)–(4.14) and the triangle inequality. \square

Remark 4.8. The estimate (4.10) indicates that, up to an $O(H + \rho)$ error, the approximation of (\bar{y}, \bar{p}) by $(\bar{y}_{H,k}^{\text{ms},h}, \bar{p}_{H,k}^{\text{ms},h})$ in the energy norm is as good as the fine scale approximation by $(\bar{y}_{h,\rho}, \bar{p}_{h,\rho})$. By comparing (3.39) with (4.10), we can also say that up to the fine scale error the performance of the multiscale finite element method (with respect to the energy norm) on coarse meshes is similar to the performance of standard finite element methods for problems with smooth coefficients on convex domains.

5. NUMERICAL RESULTS

In this section we report the numerical results of two examples, one with highly heterogeneous coefficients and one with highly oscillatory coefficients. The domain is the unit square $\Omega = (0, 1) \times (0, 1)$ for both examples, and we use the Q_1 element on uniform rectangular meshes. The regularization parameter γ is taken to be 1.

The objective function in our computations is given by

$$(5.1) \quad \tilde{J}(y, u) = \frac{1}{2} (\|y\|_{L_2(\Omega)}^2 + \gamma \|u\|_{L_2(\Omega)}^2) - \int_{\Omega} yy_d dx$$

that differs from $J(y, u)$ by the constant $\|y_d\|_{L_2(\Omega)}^2/2$.

The fine scale solution (\bar{y}_h, \bar{u}_h) (where $\mathcal{T}_\rho = \mathcal{T}_h$) is computed by using the primal-dual interior point method in the PETSc/TAO library with 20 processors on the SuperMIC supercomputer at Louisiana State University. Each compute node is equipped with two 2.8GHz 10-Core Ivy Bridge-EP E5-2680 Xeon 64-bit Processors, two Intel Xeon Phi 7120P Coprocessors, 64GB DDR3 1866MHz Ram, 500GB HD, 56 Gigabit/sec Infiniband network interface, and 1 Gigabit Ethernet network interface.

The DD-LOD solution $(\bar{y}_{H,k}^{ms,h}, \bar{u}_H)$ (with $\mathcal{T}_\rho = \mathcal{T}_H$) is computed by using the quadprog algorithm in MATLAB on a Lenovo Thinkpad X1 Carbon laptop with a 12th Gen Intel(R) Core(TM) i7-1260P processor, 4.70 GHz Max Turbo Frequency, an 18MB Intel(R) Smart Cache and 32 GB of RAM.

Example 5.1 (Highly Heterogeneous Coefficients). The coefficient matrix for this example is given by

$$\mathcal{A} = \begin{bmatrix} \mathcal{A}_{11} & \mathbf{0} \\ \mathbf{0} & \mathcal{A}_{22} \end{bmatrix},$$

where \mathcal{A}_{11} and \mathcal{A}_{22} are piecewise constant matrices with respect to a 40×40 uniform rectangular subdivision of Ω . The values of \mathcal{A}_{11} and \mathcal{A}_{22} on each square of the subdivision are randomly generated and range between 1 and 1350 (cf. Figure 5.1).

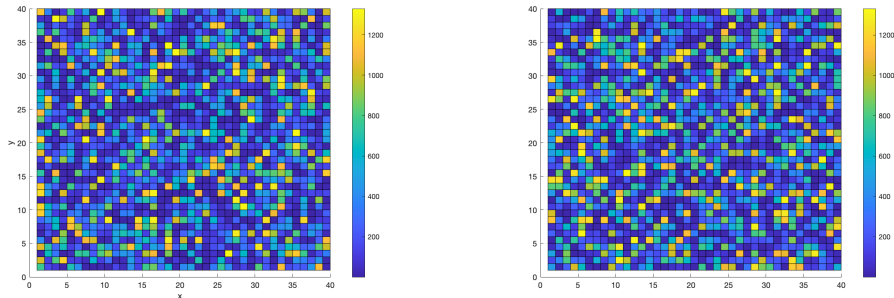


FIGURE 5.1. \mathcal{A}_{11} (left) and \mathcal{A}_{22} (right)

We choose $y_d = 1$ and the control constraints are given by $\phi_1(x) = 0.0002x_1 - 0.0001$ and $\phi_2(x) = 0.0002x_2 + 0.0001$ (cf. Figure 5.2).

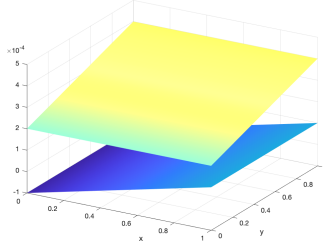


FIGURE 5.2. Graphs of the control constraints ϕ_1 and ϕ_2 for Example 5.1.

We take $h = 1/320$ for the fine scale solution (\bar{y}_h, \bar{u}_h) . In the first set of experiments we take $H = 1/10, 1/20, 1/40, 1/80$ for the DD-LOD solution $(\bar{y}_{H,k}^{ms,h}, \bar{u}_H)$ with $\mathcal{T}_\rho = \mathcal{T}_H$. The number of iterations k used in the solution of the corrector equation equals $\lceil -3 \ln H \rceil$ for $H = 1/10, 1/20$ and $1/40$, and equals $\lceil -6 \ln H \rceil$ for $H = 1/80$. The relative errors for the approximation of the standard finite element solution (\bar{y}_h, \bar{u}_h) by the multiscale finite element solution $(\bar{y}_{H,k}^{ms,h}, \bar{u}_H)$ are presented in Figure 5.3.

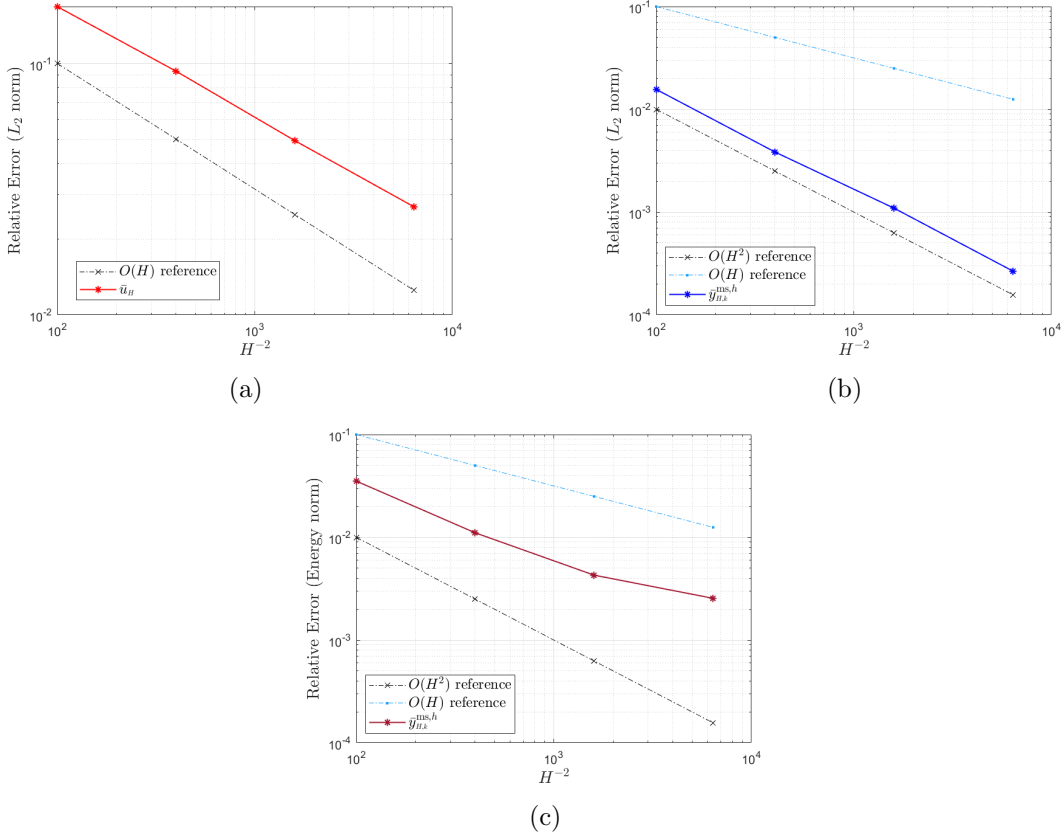


FIGURE 5.3. (a) relative L_2 error of \bar{u}_H , (b) relative L_2 error of $\bar{y}_{H,k}^{ms,h}$ and (c) relative energy error of $\bar{y}_{H,k}^{ms,h}$ for Example 5.1 with $H = 1/10, 1/20, 1/40, 1/80$.

The $O(H)$ convergence of \bar{u}_H predicted by Theorem 4.5 is observed. The convergence of $\bar{y}_{H,k}^{\text{ms},h}$ in the L_2 norm is $O(H^2)$, which is better than the $O(H)$ convergence predicted by Theorem 4.5. It should be noted that the error estimate in (4.3) concerns the approximation of (\bar{y}, \bar{u}) by $(\bar{y}_{H,k}^{\text{ms},h}, \bar{u}_H)$, and the results reported in Figure 5.3 measure the approximation of (\bar{y}_h, \bar{u}_h) by $(\bar{y}_{H,k}^{\text{ms},h}, \bar{u}_H)$. The convergence of $\bar{y}_{H,k}^{\text{ms},h}$ in the energy norm is $O(H)$, which agrees with Theorem 4.7.

For this example, the value of the modified cost function \tilde{J} in (5.1) is -3.60479×10^{-8} for the fine scale standard finite element solution (\bar{y}_h, \bar{u}_h) . The values of $\tilde{J}(\bar{y}_{H,k}^{\text{ms},h}, \bar{u}_H)$ are displayed in Table 5.1. The order of convergence of $\tilde{J}(\bar{y}_{H,k}^{\text{ms},h}, \bar{u}_H)$ is roughly $O(H^2)$, which is consistent with Theorem 4.5.

H	$\tilde{J}(\bar{y}_{H,k}^{\text{ms},h}, \bar{u}_H)$
1/10	-3.55321×10^{-8}
1/20	-3.59107×10^{-8}
1/40	-3.60102×10^{-8}
1/80	-3.60372×10^{-8}

TABLE 5.1. Values of $\tilde{J}(\bar{y}_{H,k}^{\text{ms},h}, \bar{u}_H)$ for Example 5.1.

We compare the graphs of \bar{y}_h and $\bar{y}_{H,k}^{\text{ms},h}$ (with $H = 1/20$) in Figure 5.4, and the graphs of \bar{u}_h and \bar{u}_H (with $H = 1/20$) in Figure 5.5.

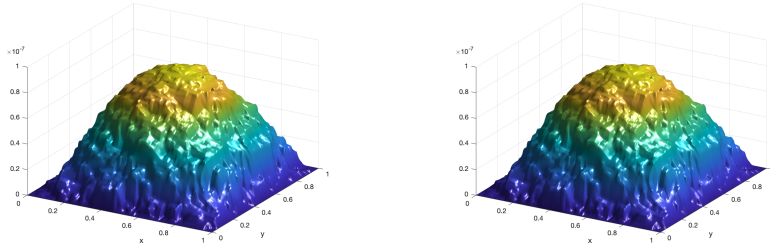


FIGURE 5.4. Graph of \bar{y}_h (left) and graph of $\bar{y}_{H,k}^{\text{ms},h}$ (right, with $H = 1/20$) for Example 5.1.

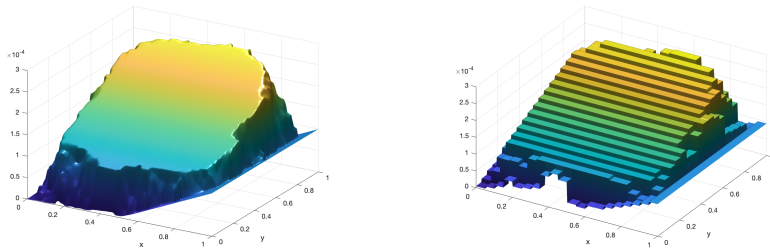


FIGURE 5.5. Graph of \bar{u}_h (left) and graph of \bar{u}_H (right, with $H = 1/20$) for Example 5.1.

The active sets for \bar{u}_h and \bar{u}_H (with $H = 1/20$) are depicted in Figure 5.6 and Figure 5.7.

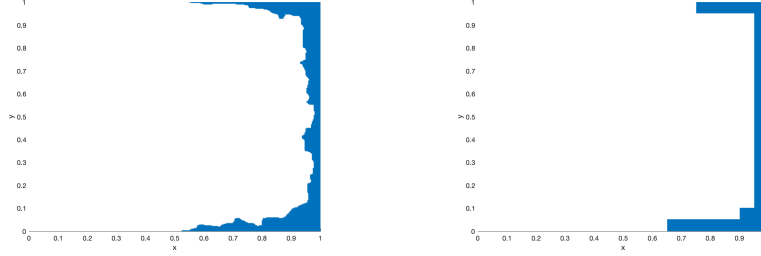


FIGURE 5.6. Active sets for ϕ_1 for Example 5.1: \bar{u}_h (left) and \bar{u}_H (right, $H = 1/20$).

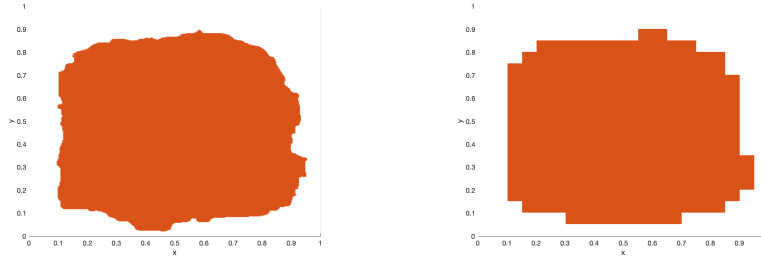


FIGURE 5.7. Active sets for ϕ_2 for Example 5.1: \bar{u}_h (left) and \bar{u}_H (right, $H = 1/20$).

The computation of the fine scale standard finite element solution (\bar{y}_h, \bar{u}_h) of the discrete optimization problem takes $3.90 \times 10^{+1}$ seconds by using the PETS_c/TAO library with 20 processors. The computational time (in seconds) for $(\bar{y}_{H,k}^{\text{ms},h}, \bar{u}_H)$ using MATLAB on a laptop are presented in Table 5.2 for $H = 1/10, 1/20, 1/40$.

H	Time
1/10	1.26×10^{-2}
1/20	1.74×10^{-1}
1/40	$1.04 \times 10^{+1}$

TABLE 5.2. Computational time in seconds for $(\bar{y}_{H,k}^{\text{ms},h}, \bar{u}_H)$ (Example 5.1).

For $H = 1/20$, the DD-LOD solution $(\bar{y}_{H,k}^{\text{ms},h}, \bar{u}_H)$ yields a reasonable approximation of (\bar{y}_h, \bar{u}_h) (cf. Figures 5.4–5.7) and its computation is more than 100 times faster than the computation of (\bar{y}_h, \bar{u}_h) .

In the second set of experiments we take $H = 1/20$ and $\rho = 1/40, 1/80, 1/160$ for the DD-LOD solution $(\bar{y}_{H,k}^{\text{ms},h}, \bar{u}_\rho)$. In view of Theorem 4.5 and Theorem 4.7, we expect these approximate solutions will improve over the approximate solution $(\bar{y}_{H,k}^{\text{ms},h}, \bar{u}_H)$ with $H = 1/20$ and $\mathcal{T}_\rho = \mathcal{T}_H$ obtained in the first set of experiments. This is confirmed by comparing the

values of the cost function \tilde{J} in Table 5.3 with the value $\tilde{J}(\bar{y}_h, \bar{u}_h) = -3.60479 \times 10^{-8}$ for the fine scale solution. The number of significant digits increases from 2 to 4 as ρ decreases from $1/20$ to $1/160$.

ρ	$\tilde{J}(\bar{y}_{H,k}^{\text{ms},h}, \bar{u}_\rho)$
$1/20$	-3.59107×10^{-8}
$1/40$	-3.60090×10^{-8}
$1/80$	-3.60357×10^{-8}
$1/160$	-3.60431×10^{-8}

TABLE 5.3. Values of $\tilde{J}(\bar{y}_{H,k}^{\text{ms},h}, \bar{u}_\rho)$ with $H = 1/20$ and various ρ for Example 5.1.

We can also visualize the improvement due to a smaller ρ by comparing the graph of the fine scale solution \bar{u}_h for the optimal control and the graph of the DD-LOD solution \bar{u}_ρ for the optimal control (with $H = 1/20$ and $\rho = 1/160$) in Figure 5.8. They are hardly distinguishable, which is not the case for the graphs in Figure 5.5.

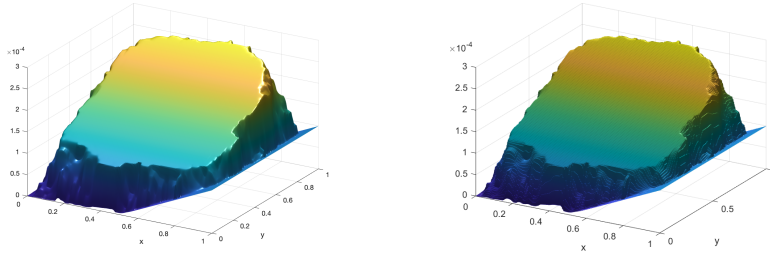


FIGURE 5.8. Graph of \bar{u}_h (left) and graph of \bar{u}_ρ (right, with $H = 1/20$ and $\rho = 1/160$.) for Example 5.1.

This is also true for the active sets, where the ones for the fine scale solution \bar{u}_h and the ones for the DD-LOD solution \bar{u}_ρ (with $H = 1/20$ and $\rho = 1/160$) are almost identical in Figure 5.9 and Figure 5.10.

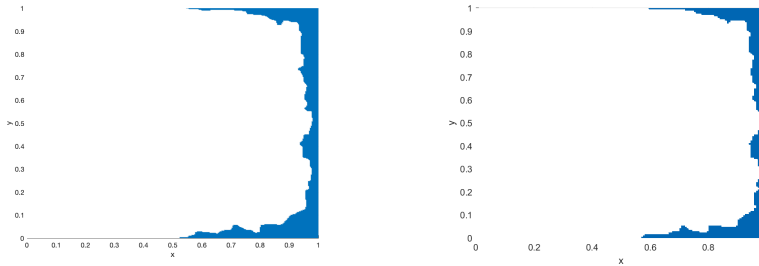


FIGURE 5.9. Active sets for ϕ_1 for Example 5.1: \bar{u}_h (left) and \bar{u}_ρ (right, $H = 1/20$ and $\rho = 1/160$).

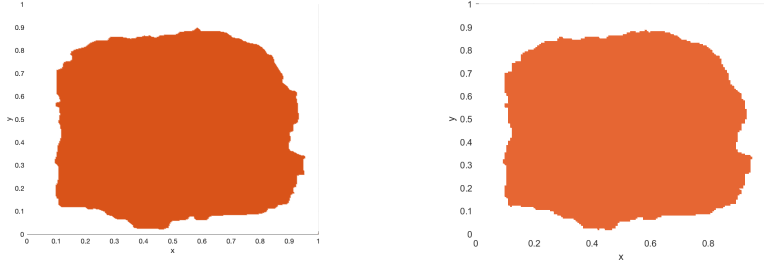


FIGURE 5.10. Active sets for ϕ_2 for Example 5.1: \bar{u}_h (left) and \bar{u}_ρ (right, $H = 1/20$ and $\rho = 1/160$).

Example 5.2 (Highly Oscillatory Coefficients). The coefficient matrix for this example is given by

$$\mathcal{A} = \begin{bmatrix} c(x) & \mathbf{0} \\ \mathbf{0} & c(x) \end{bmatrix},$$

where

$$c(x) = \frac{2 + 1.8 \sin\left(\frac{2\pi x_1}{\epsilon}\right)}{2 + 1.8 \sin\left(\frac{2\pi x_2}{\epsilon}\right)} + \frac{2 + \sin\left(\frac{2\pi x_2}{\epsilon}\right)}{2 + 1.8 \sin\left(\frac{2\pi x_1}{\epsilon}\right)}$$

with $\epsilon = 0.025$. This choice of coefficients originates from the pioneering work [23] in numerical homogenization.

We choose $y_d = -1$ and the control constraints are given by $\phi_1(x) = -0.01x_1 - 0.005$ and $\phi_2(x) = 0.0007x_2 - 0.005$ (cf. Figure 5.11).

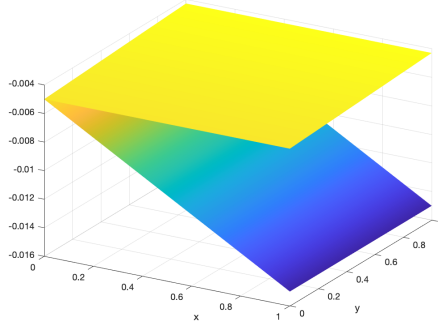


FIGURE 5.11. Graphs of the control constraints ϕ_1 and ϕ_2 for Example 5.2.

We take $h = 1/320$ for the fine scale solution (\bar{y}_h, \bar{u}_h) . In the first set of experiments we compute the DD-LOD solution $(\bar{y}_{H,k}^{\text{ms},h}, \bar{u}_H)$ for $H = 1/10, 1/20, 1/40, 1/80$ (with $\mathcal{T}_\rho = \mathcal{T}_H$). The number of iterations k used in the solution of the corrector equation equals $\lceil -3 \ln H \rceil$ for all H . The relative errors for the approximation of the fine scale standard finite element solution (\bar{y}_h, \bar{u}_h) by the multiscale finite element solution $(\bar{y}_{H,k}^{\text{ms},h}, \bar{u}_H)$ are presented in Figure 5.12. The $O(H)$ convergence is observed for both \bar{u}_H and $\bar{y}_{H,k}^{\text{ms},h}$, which agrees with Theorem 4.5 and Theorem 4.7.

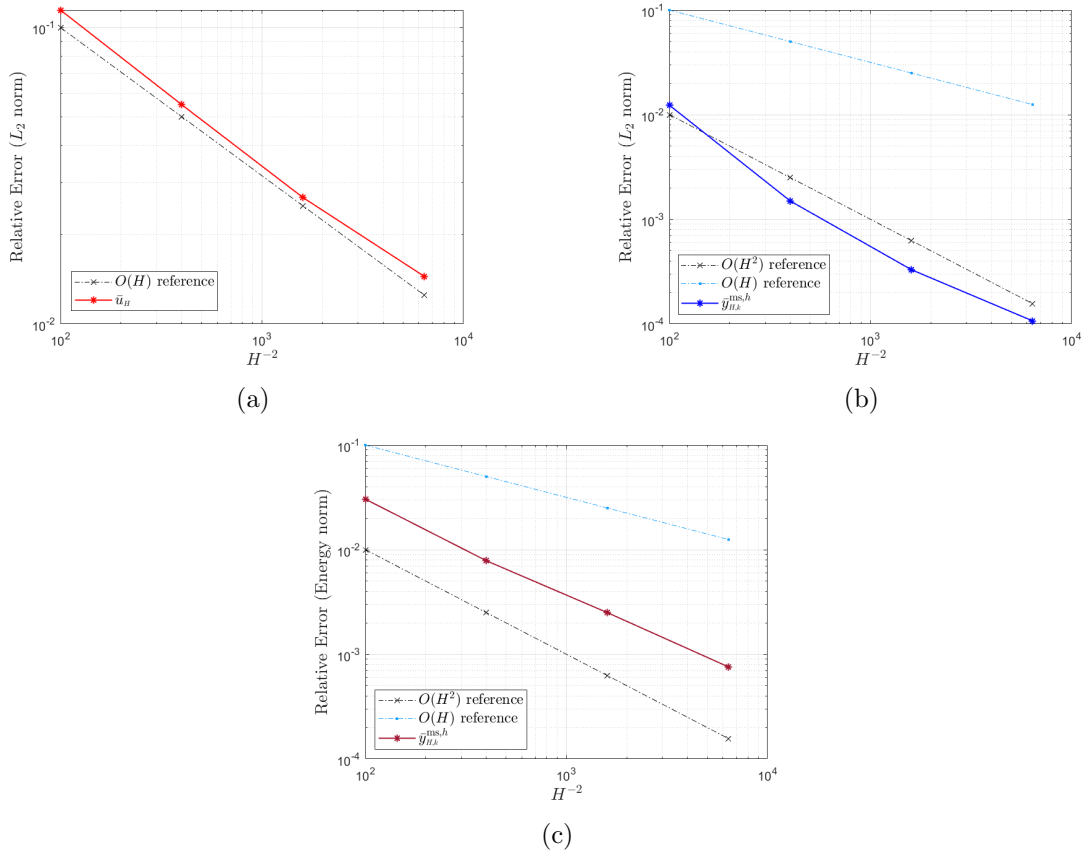


FIGURE 5.12. (a) relative L_2 error of \bar{u}_H , (b) relative L_2 error of $\bar{y}_{H,k}^{\text{ms},h}$ and (c) relative energy error of $\bar{y}_{H,k}^{\text{ms},h}$ for Example 5.2 with $H = 1/10, 1/20, 1/20, 1/80$.

For this example, the value of the modified cost function \tilde{J} in (5.1) is -8.29631×10^{-5} for the fine scale standard finite element solution (\bar{y}_h, \bar{u}_h) . The values of $\tilde{J}(\bar{y}_{H,k}^{\text{ms},h}, \bar{u}_H)$ are displayed in Table 5.4. The $O(H^2)$ convergence of $\tilde{J}(\bar{y}_{H,k}^{\text{ms},h}, \bar{u}_H)$ also agrees with Theorem 4.5.

H	$\tilde{J}(\bar{y}_{H,k}^{\text{ms},h}, \bar{u}_H)$
1/10	-8.22171×10^{-5}
1/20	-8.28313×10^{-5}
1/40	-8.29343×10^{-5}
1/80	-8.29550×10^{-5}

TABLE 5.4. Values of $\tilde{J}(\bar{y}_{H,k}^{\text{ms},h}, \bar{u}_H)$ for Example 5.2.

We compare the graphs of \bar{y}_h and $\bar{y}_{H,k}^{\text{ms},h}$ (with $H = 1/20$) in Figure 5.13, and the graphs of \bar{u}_h and \bar{u}_H (with $H = 1/20$) in Figure 5.14. The active sets for \bar{u}_h and \bar{u}_H (with $H = 1/20$) are depicted in Figure 5.15 and Figure 5.16.

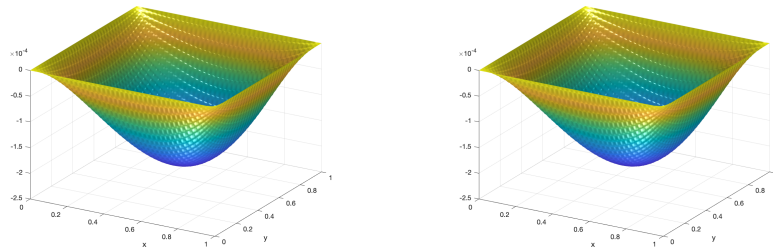


FIGURE 5.13. Graph of \bar{y}_h (left) and graph of $\bar{y}_{H,k}^{ms,h}$ (right, $H = 1/20$) for Example 5.2.

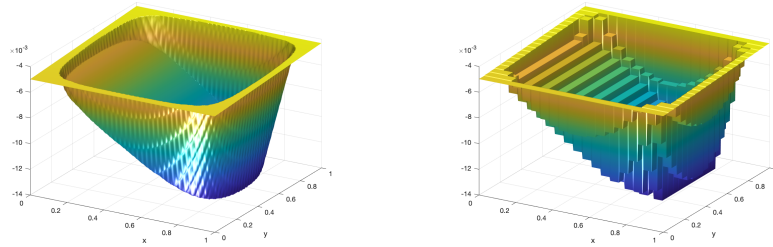


FIGURE 5.14. Graph of \bar{u}_h (left) and graph of \bar{u}_H (right, $H = 1/20$) for Example 5.2.

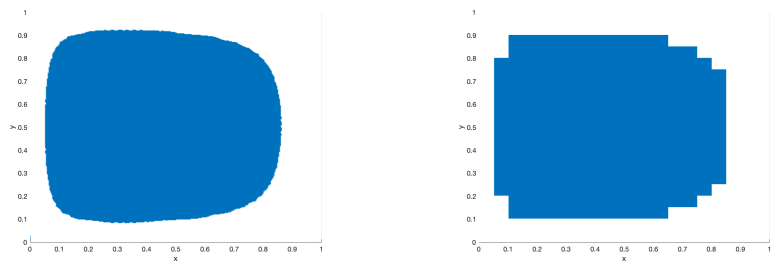


FIGURE 5.15. Active set for ϕ_1 for Example 5.2: \bar{u}_h (left) and \bar{u}_H (right, $H = 1/20$).

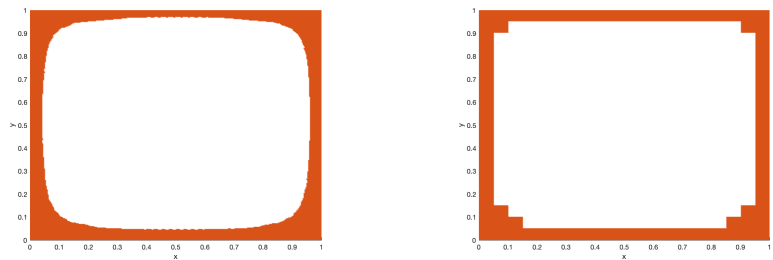


FIGURE 5.16. Active set for ϕ_2 for Example 5.2: \bar{u}_h (left) and \bar{u}_H (right, $H = 1/20$).

The computation of the fine scale standard finite element solution (\bar{y}_h, \bar{u}_h) of the discrete optimization problem takes $4.36 \times 10^{+1}$ seconds by using the PETSc/TAO library with

20 processors. The computational time (in seconds) for $(\bar{y}_{H,k}^{\text{ms},h}, \bar{u}_H)$ using MATLAB on a laptop are presented in Table 5.5 for $H = 1/10, 1/20, 1/40$. For $H = 1/20$, the DD-LOD solution $(\bar{y}_{H,k}^{\text{ms},h}, \bar{u}_H)$ is a reasonable approximation of (\bar{y}_h, \bar{u}_h) (cf. Figures 5.13–5.16) and its computation is more than 200 times faster than the computation of (\bar{y}_h, \bar{u}_h) .

H	Time
1/10	1.71×10^{-2}
1/20	1.27×10^{-1}
1/40	$1.40 \times 10^{+1}$

TABLE 5.5. Computational time in seconds for $(\bar{y}_{H,k}^{\text{ms},h}, \bar{u}_H)$ for Example 5.2.

In the second set of experiments we take $H = 1/20$ and test the improved approximation by the DD-LOD solution $(\bar{y}_{H,k}^{\text{ms},h}, \bar{u}_\rho)$ for $\rho = 1/40, 1/80, 1/160$ that is predicted by the estimates in Theorem 4.5 and Theorem 4.7. This improvement can be observed by comparing the values of the cost function \tilde{J} in Table 5.6 with the value $\tilde{J}(\bar{y}_h, \bar{u}_h) = -8.29631 \times 10^{-5}$ for the fine scale solution. The number of significant digits improves from 2 to 3 as ρ decreases from 1/20 to 1/160.

ρ	$\tilde{J}(\bar{y}_{H,k}^{\text{ms},h}, \bar{u}_\rho)$
1/20	-8.28313×10^{-5}
1/40	-8.29252×10^{-5}
1/80	-8.29448×10^{-5}
1/160	-8.29510×10^{-5}

TABLE 5.6. Values of $\tilde{J}(\bar{y}_{H,k}^{\text{ms},h}, \bar{u}_\rho)$ with $H = 1/20$ and various ρ for Example 5.2.

The improvement can also be visualized through a comparison of the graphs of the fine scale solution \bar{u}_h and the DD-LOD solution \bar{u}_ρ (with $H = 1/20$ and $\rho = 1/160$) in Figure 5.17. They are almost identical, which is not the case in Figure 5.14.

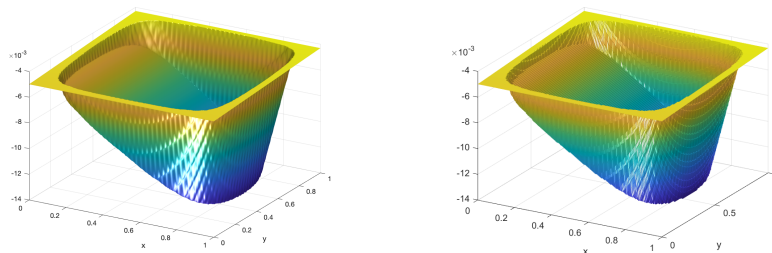


FIGURE 5.17. Graph of \bar{u}_h (left) and graph of \bar{u}_ρ (right, $H = 1/20$, $\rho = 1/160$) for Example 5.2.

We can also observe the improvement due to smaller ρ by comparing the active sets depicted in Figure 5.18 and Figure 5.19. These sets are almost identical, which is not the case in Figure 5.15 and Figure 5.16.

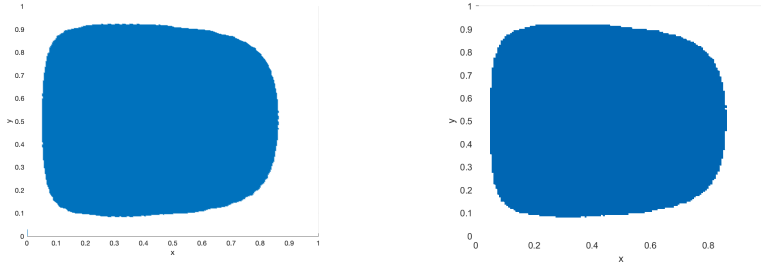


FIGURE 5.18. Active set for ϕ_1 for Example 5.2: \bar{u}_h (left) and \bar{u}_ρ (right, $H = 1/20$ and $\rho = 1/160$).

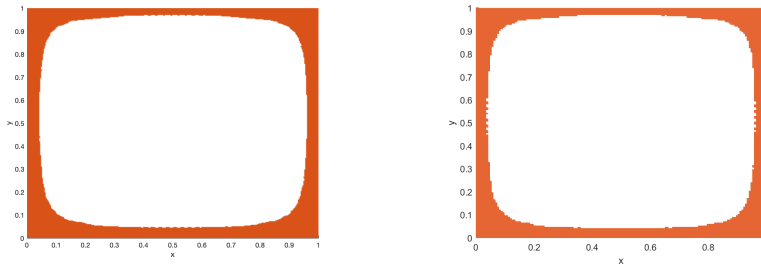


FIGURE 5.19. Active set for ϕ_2 for Example 5.2: \bar{u}_h (left) and \bar{u}_ρ (right, $H = 1/20$ and $\rho = 1/160$).

6. CONCLUDING REMARKS

We have constructed and analyzed a multiscale finite element method for the optimal control problem defined by (1.1)–(1.5). We showed that the approximate solution obtained by the DD-LOD finite element method on the coarse mesh \mathcal{T}_H is, up to an $O(H^2 + \rho)$ term for the L_2 error and an $O(H + \rho)$ term for the energy error, as good as the approximate solution obtained by a standard finite element method on a fine mesh \mathcal{T}_h . Alternatively we can say that up to the fine scale error the performance of the DD-LOD method is as good as standard finite element methods for smooth problems.

The DD-LOD multiscale finite element method is one of the simplest multiscale finite element methods in terms of construction and analysis. There is inherent parallelism in the construction of the DD-LOD finite element space that comes from domain decomposition so that it can readily benefit from high performance computing (cf. [6]), and its analysis only requires basic knowledge in finite element methods, domain decomposition methods and numerical linear algebra. After a multiscale basis has been computed off-line, the on-line solution with the coarse scale DD-LOD finite element method is fast. The multiscale finite

element method is particularly useful for applications where the optimal control problem has to be solved repeatedly for different y_d , ϕ_1 and ϕ_2 .

We note that the error estimates in Theorem 3.3 and Theorem 3.5 are applicable to any subspace V_* of $H_0^1(\Omega)$. The key is to have good error estimates for the Galerkin solution of (4.1). In particular, we can take V_* to be the LOD multiscale finite element spaces in [33, 21, 22] and arrive at similar results. Note that the LOD methods in [33, 21] are suitable for problems with high contrast.

We can also take V_* to be the multiscale finite element space V_h from [23, 24, 15] for problems with highly oscillatory and periodic coefficients (such as the problem in Example 5.2), where h stands for the coarse mesh size. The corresponding L_2 error estimate then takes the form

$$\|\bar{y} - \bar{y}_{h,\rho}\|_{L_2(\Omega)} + \|\bar{u} - \bar{u}_{h,\rho}\|_{L_2(\Omega)} + \|\bar{p} - \bar{p}_{h,\rho}\|_{L_2(\Omega)} \leq C \left(h^2 + \epsilon + \frac{\epsilon}{h} + \rho \right),$$

where ϵ ($< h$) is the parameter for the small scale, and the positive constant C only depends on $\|y_d\|_{L_2(\Omega)}$, $\|\phi_1\|_{H^1(\Omega)}$, $\|\phi_2\|_{H^1(\Omega)}$, γ^{-1} , α^{-1} and the shape regularities of \mathcal{T}_h and \mathcal{T}_ρ .

Similarly, the multiscale finite element methods in [3, 9] can also be analyzed by Theorem 3.3, Theorem 3.5 and the estimates in [32, 11].

ACKNOWLEDGEMENTS

Portions of this research were conducted with high performance computing resources provided by Louisiana State University (<http://www.hpc.lsu.edu>).

FUNDING

This work was supported in part by the National Science Foundation under Grant No. DMS-19-13035 and Grant No. DMS-22-08404.

DATA AVAILABILITY

The datasets generated during and/or analyzed during the current study are available from the corresponding author on reasonable request.

REFERENCES

- [1] R.A. Adams and J.J.F. Fournier. *Sobolev Spaces (Second Edition)*. Academic Press, Amsterdam, 2003.
- [2] R. Altmann, P. Henning, and D. Peterseim. Numerical homogenization beyond scale separation. *Acta Numer.*, 30:1–86, 2021.
- [3] T.S. Au Yeung and E. Chung. Multiscale model reduction for a class of optimal control problems with highly oscillatory coefficients. In S.C. Brenner, E. Chung, A. Klawonn, F. Kwok, J. Xu, and J. Zou, editors, *Lecture Notes in Computational Science and Engineering 145*, pages 3–15. Springer, 2022.
- [4] I. Babuška and J.E. Osborn. Can a finite element method perform arbitrarily badly? *Math. Comp.*, 69:443–462, 2000.
- [5] S.C. Brenner, J.C. Garay, and L.-Y. Sung. Additive Schwarz preconditioners for a localized orthogonal decomposition method. *Electron. Trans. Numer. Anal.*, 54:234–255, 2021.
- [6] S.C. Brenner, J.C. Garay, and L.-Y. Sung. Multiscale finite element methods for an elliptic optimal control problem with rough coefficients. *J. Sci. Comput.*, 91:Paper No. 76, 2022.
- [7] S.C. Brenner and L.R. Scott. *The Mathematical Theory of Finite Element Methods (Third Edition)*. Springer-Verlag, New York, 2008.

- [8] Y. Chen, Y. Huang, W. Liu, and N. Yan. A mixed multiscale finite element method for convex optimal control problems with oscillating coefficients. *Comput. Math. Appl.*, 70:297–313, 2015.
- [9] Y. Chen, X. Liu, J. Zeng, and L. Zhang. Optimal control for multiscale elliptic equations with rough coefficients. *J. Comput. Math.*, 41:842–866, 2023.
- [10] Z. Chen and T.Y. Hou. A mixed multiscale finite element method for elliptic problems with oscillating coefficients. *Math. Comp.*, 72:541–576, 2003.
- [11] E.T. Chung, Y. Efendiev, and W.T. Leung. Constraint energy minimizing generalized multiscale finite element method. *Comput. Methods Appl. Mech. Engrg.*, 339:298–319, 2018.
- [12] P.G. Ciarlet. *The Finite Element Method for Elliptic Problems*. North-Holland, Amsterdam, 1978.
- [13] M. Dauge. *Elliptic Boundary Value Problems on Corner Domains*, Lecture Notes in Mathematics 1341. Springer-Verlag, Berlin-Heidelberg, 1988.
- [14] W. E and B. Engquist. The heterogeneous multiscale methods. *Commun. Math. Sci.*, 1:87–132, 2003.
- [15] Y. Efendiev and T.Y. Hou. *Multiscale Finite Element Methods*. Springer, New York, 2009.
- [16] I. Ekeland and R. T emam. *Convex Analysis and Variational Problems*. Classics in Applied Mathematics. Society for Industrial and Applied Mathematics, Philadelphia, PA, 1999.
- [17] R.S. Falk. Approximation of a class of optimal control problems with order of convergence estimates. *J. Math. Anal. Appl.*, 44:28–47, 1973.
- [18] L. Ge, N. Yan, L. Wang, W. Liu, and D. Yang. Heterogeneous multiscale method for optimal control problem governed by elliptic equations with highly oscillatory coefficients. *J. Comput. Math.*, 36, 2018.
- [19] D. Gilbarg and N.S. Trudinger. *Elliptic Partial Differential Equations of Second Order*. Classics in Mathematics. Springer-Verlag, Berlin, 2001.
- [20] P. Grisvard. *Elliptic Problems in Non Smooth Domains*. Pitman, Boston, 1985.
- [21] F. Hellman and A. M alqvist. Contrast independent localization of multiscale problems. *Multiscale Model. Simul.*, 15:1325–1355, 2017.
- [22] P. Henning and D. Peterseim. Oversampling for the multiscale finite element method. *Multiscale Model. Simul.*, 11:1149–1175, 2013.
- [23] T.Y. Hou and X.-H. Wu. A multiscale finite element method for elliptic problems in composite materials and porous media. *J. Comput. Phys.*, 134:169–189, 1997.
- [24] T.Y. Hou, X.-H. Wu, and Z. Cai. Convergence of a multiscale finite element method for elliptic problems with rapidly oscillating coefficients. *Math. Comp.*, 68:913–943, 1999.
- [25] D. Kinderlehrer and G. Stampacchia. *An Introduction to Variational Inequalities and Their Applications*. Society for Industrial and Applied Mathematics, Philadelphia, 2000.
- [26] R. Kornhuber, D. Peterseim, and H. Yserentant. An analysis of a class of variational multiscale methods based on subspace decomposition. *Math. Comp.*, 87:2765–2774, 2018.
- [27] J.-L. Lions. *Optimal Control of Systems Governed by Partial Differential Equations*. Springer-Verlag, New York, 1971.
- [28] J. Liu, L. Cao, and N. Yan. Multiscale asymptotic analysis and computation of optimal control for elliptic systems with constraints. *SIAM J. Numer. Anal.*, 51:1978–2004, 2013.
- [29] A. M alqvist and D. Peterseim. Localization of elliptic multiscale problems. *Math. Comp.*, 83:2583–2603, 2014.
- [30] A. M alqvist and D. Peterseim. *Numerical Homogenization by Localized Orthogonal Decomposition*. SIAM, Philadelphia, 2021.
- [31] V. Maz’ya and J. Rossmann. *Elliptic Equations in Polyhedral Domains*. American Mathematical Society, Providence, RI, 2010.
- [32] H. Owhadi, L. Zhang, and L. Berlyand. Polyharmonic homogenization, rough polyharmonic splines and sparse super-localization. *ESAIM Math. Model. Numer. Anal.*, 48:517–552, 2014.
- [33] D. Peterseim and R. Scheichl. Robust numerical upscaling of elliptic multiscale problems at high contrast. *Comput. Methods Appl. Math.*, 16:579–603, 2016.
- [34] Y. Saad. *Iterative Methods for Sparse Linear Systems*. SIAM, Philadelphia, 2003.
- [35] A. Toselli and O.B. Widlund. *Domain Decomposition Methods - Algorithms and Theory*. Springer, New York, 2005.

- [36] F. Tröltzsch. *Optimal Control of Partial Differential Equations*. American Mathematical Society, Providence, RI, 2010.

DEPARTMENT OF MATHEMATICS AND CENTER FOR COMPUTATION & TECHNOLOGY, LOUISIANA STATE UNIVERSITY, BATON ROUGE, LA 70803, USA

Email address: `brenner@math.lsu.edu`

INSTITUTE OF MATHEMATICS, UNIVERSITÄT AUGSBURG, 86159 AUGSBURG, GERMANY

Email address: `jose.garay.fernandez@uni-a.de`

DEPARTMENT OF MATHEMATICS AND CENTER FOR COMPUTATION & TECHNOLOGY, LOUISIANA STATE UNIVERSITY, BATON ROUGE, LA 70803, USA

Email address: `sung@math.lsu.edu`